Optimization of Spark Plasma Sintering Parameters Using the Taguchi Method for Developing Mg-Based Composites

MURAD ALI,[1] M.A. HUSSEIN [iD],[2,3] and N. AL-AQEELI[1]

1.—Department of Mechanical Engineering, King Fahd University of Petroleum and Minerals (KFUPM), Dhahran 31261, Saudi Arabia. 2.—Center of Research Excellence in Corrosion, King Fahd University of Petroleum and Minerals'(KFUPM), Dhahran 31261, Saudi Arabia. 3.—e-mail: mahussein@kfupm.edu.sa

A magnesium-based metal matrix composite incorporated with 2.5 wt.% TiB_2 has been fabricated using spark plasma sintering for the first time. The Taguchi design approach was used to analyze the significant influences of sintering parameters such as the temperature, pressure, and time on the physical and mechanical properties of Mg-based composites. Analysis of variance was used to investigate the effect of each sintering parameter. X-ray diffraction and field-emission scanning electron microscopy equipped with energy-dispersive x-ray spectroscopy were used for structure and microstructure analysis. Rockwell hardness (HR) and Vickers hardness (HV) were used to evaluate the mechanical properties of the composite. The results showed that, in the case of microhardness, all the sintering parameters were controlling factors, and the sintering temperature was the most significant factor. The maximum values obtained for the densification, Rockwell hardness, and Vickers hardness were 100%, 62.18 HR, and 58.6 HV, respectively.

INTRODUCTION

Magnesium-based materials have had a significant impact on various industrial sectors, including the automobile and aerospace industries, due to the low density (1.738 g/cm^3), high strength-to-weight ratio, and stiffness of Mg.[1,2] However, Mg has a comparatively low elastic modulus, low strength, insufficient ductility, high creep, high wear, low corrosion resistance, and fatigue that could limit its extensive industrial use.[2] Nevertheless, many efforts have been made by researchers to fabricate Mg-based alloys or composites with Cu, Ti, Al, TiO_2, ZnO, Al_2O_3, ZrO_2, and TiB_2 to achieve desired mechanical properties and enhanced ductility.[3–12] Magnesium is one of the most suitable biocompatible and biodegradable elements. Therefore, Mg-based materials have great potential for use in clinical applications.[13,14] Cobalt-chromium alloys, austenitic stainless steel, and Ti-based materials are extensively used in medical applications. However, the use of these materials results in toxic products that are harmful to the patient and require costly postsurgery care after the healing process.[15–22] One way to achieve a suitable Mg-based material with adequate mechanical properties for biomedical applications is to incorporate a suitable reinforcement into the Mg matrix. The resulting improvement in the mechanical properties of the Mg matrix is highly dependent on achieving a uniform distribution of the reinforcement.[23,24] Different methods have been reported for fabricating Mg-based composites, such as liquid infiltration,[6] stir casting,[25–27] squeeze casting,[28] mechanical alloying,[29–32] and powder metallurgy processes.[29,30,33–39] In powder metallurgy, the reinforcement can be well distributed within the matrix in the absence of an interaction or with a minimum interaction between the matrix and reinforcement.

After the powder has been mixed, consolidation of the powder mixture can be carried out using a novel sintering technique called spark plasma sintering (SPS). In this technique, the powder material is heated and compacted simultaneously to achieve the maximum density and minimum grain growth due to the high heating rate, in a reduced experimental time compared with conventional sintering techniques.[40,41] SPS can offer a lower sintering temperature and shorter sintering time, resulting in improved mechanical properties compared with the

(Published online January 14, 2020)

conventional sintering technique. Researchers have used SPS extensively in the fabrication of various metals, ceramics, and their alloys and composites.[42–45] However, there is a scarcity of literature on the use of SPS for Mg-based composites. Nguyen et al. successfully developed an Mg-based in situ composite of Mg-ZnO using SPS, which exhibited improved corrosion resistance in Hank's solution.[46] This kind of improvement is generally difficult to achieve by using conventional sintering techniques.[45,47]

Titanium diboride (TiB$_2$) is a ceramic reinforcement with high melting temperature (2790°C), high Rockwell hardness (86 HRA), high Vickers hardness (960 HV), high elastic modulus of 530 GPa, and excellent thermal stability.[48] As a result of these excellent properties, TiB$_2$ has a wide range of applications in erosion, corrosion, abrasion, and high-temperature applications.[49] Recently, a Mg matrix was reinforced with TiB$_2$ to enhance its mechanical properties, making it more attractive for use in orthopedic applications. Powder metallurgy combined with the conventional sintering technique has also been used to fabricate a Mg-TiB$_2$ composite, achieving significant improvements in hardness and wear resistance.[50] Similarly, a Mg-TiB$_2$ nanocomposite was prepared by disintegrated melt deposition followed by hot extrusion, obtaining an improved compressive yield strength, compressive tensile strength, and fracture strain, and modified basal texture.[12] However, to the best of the authors' knowledge, there are no previous reports on fabrication of Mg-2.5TiB$_2$ composites by spark plasma sintering.

In view of the above prospects of Mg and TiB$_2$ materials, an attempt was made in the work described herein to study the effect of sintering parameters such as the sintering temperature (S. Temp), sintering pressure (S. Pres), and sintering time (S. Time) on the mechanical and physical properties of Mg-2.5TiB$_2$ composites, namely their microhardness, macrohardness, and density. The resultant mechanical and physical properties of the Mg-2.5TiB$_2$ composite are a combined effect of more than one sintering parameter and their interactions. Thus, a statistical design approach called the Taguchi method was used effectively to determine the significance level of the effect of each parameter on the composite properties.

EXPERIMENTAL PROCEDURES

Design of Experiments

The design of experiments (DOE) method, which includes the Taguchi method, response surface method, and factorial design, is now widely used to overcome the limitations of conventional optimization techniques.[51] Based on a fractional factorial design, the Taguchi method is widely used to optimize the process parameters and reduce experimental time and cost,[52,53] as well as to avoid the full factorial design by carefully choosing the experimental runs.[54] The two essential tools of the Taguchi method are an orthogonal array (OA) and the signal-to-noise (S/N) ratio, where the OA is a matrix consisting of rows and columns filled with all the possible combinations of the controllable variables.[52] Meanwhile, the S/N ratio is the ratio of the sensitivity to variability; therefore, minimizing the noise effect results in maximizing the S/N ratio, which enhances the quality attributes of the product. In view of the objective function, the S/N ratio can be categorized as larger is best, nominal is best, and smaller is best.

High microhardness, macrohardness, and experimental density are desirable in the present work, thus statistical analysis was carried out with the option of higher is better. The S/N ratio for larger is best is calculated according to Eq. 1:

$$\frac{S}{N} = -10 \log \frac{1}{n} \left(\sum_{i=1}^{n} \frac{1}{y_i^2} \right), \tag{1}$$

where y_i ($i = 1, 2, \ldots, n$) are the observed average data and n is the number of observations.

Experiments were performed according to a standard orthogonal array (SOA). The orthogonal array is selected only when the number of degrees of freedom is equal to or greater than the sum of the parameters.[26–29] Three factors (S. Temp, S. Pres, and S. Time) are considered herein, each presenting three levels in the experiments, viz. 450°C, 500°C, and 550°C for S. Temp, 30 MPa, 40 MPa, and 50 MPa for S. Pres, and 5 min, 10 min, and 15 min for S. Time. An L$_9$ orthogonal array with nine rows and three columns was selected (Table I). The sintering parameters selected for the experiments were (1) S. Temp, (2) S. Pres, and (3) S. Time. The responses to be analyzed were microhardness, macrohardness, and experimental density, with the objective of larger is best, and the responses were subjected to analysis of variance (ANOVA).

Table I. Taguchi L$_9$ design orthogonal arrays

L$_9$ test sample	S. Temp (°C)	S. Pres (MPa)	S. Time (min)
1	450	30	5
2	450	40	10
3	450	50	15
4	500	30	10
5	500	40	15
6	500	50	5
7	550	30	15
8	550	40	5
9	550	50	10

Materials and Processing

Mg powder with purity > 99.8% and average particle size of < 45 μm supplied by Alfa Aesar, USA, was used as the base material. Titanium diboride (TiB_2) powder with purity of 99% and average particle size of 10 μm, as supplied by BOC Science, USA, was used as the reinforcement. A pure Mg matrix with 2.5 wt.% TiB_2 reinforcement was synthesized via a powder metallurgy processing route. A mixture of Mg and TiB_2 powders at the chosen ratio was combined using a low-energy milling machine (Fritsch Pulverisette 5) to achieve a homogeneous distribution of the reinforcement in the matrix material. The powder mixture was milled at 200 rpm for 1 h in stainless-steel vials without balls filled with Ar gas. The milled powders were consolidated (nine runs) using SPS (FCT group, System GmBH; Germany) at three levels of sintering pressure, temperature, and time, according to the L_9 orthogonal array in Table I. The milled powder mixture was loaded into a 14.8-mm-diameter graphite die with respective punches. A thin graphite sheet was inserted between the powder mixture and die wall to allow easy removal of the sample after consolidation. Additionally, this thin sheet could reduce friction between the die wall and powder. The sintering temperature during consolidation was measured by inserting a thermocouple into the middle of the die, 2 mm away from the die internal wall. The sintered samples were then cleaned of graphite by grinding and polishing. Grinding was performed with SiC paper of 180, 320, 400, 600, and 800 grit sizes. This process was followed by polishing with alumina slurry. To remove the small particles of alumina that attached to the composites during polishing, the samples were immersed in ethanol solution and ultrasonicated using a digital ultrasonic cleaner for 15 min.

Characterization

The structures of the as-received powder, milled Mg-2.5TiB_2 powder mixture, and sintered samples were characterized via x-ray diffraction (XRD) analysis using Cu K_α radiation at wavelength $\lambda = 1.54056$ Å and scan speed of 2°/min in an AXSDB Bruker device. The density of the spark-plasma-sintered Mg-2.5TiB_2 composite samples was measured using Archimedes' principle. The samples were weighed in air and then in distilled water using a digital scale with accuracy of ± 0.00001 g. An average of five values for density is reported herein. The rule-of-mixture method was used to calculate the theoretical density of the prepared composites. The distribution of the TiB_2 reinforcement and the surface morphology of the Mg-2.5TiB_2 composites were investigated. The microstructure of the spark-plasma-sintered samples was studied by field-emission scanning electron microscopy (FE-SEM) with a Schottky field-emission gun (TESCAN)

and scanning electron microscopy (SEM) with a field-emission gun (QUANTA^M FEG 250).

A Vickers hardness (HV) test was carried out using a universal hardness machine (Buehler, 60044; USA) equipped with a Vickers diamond pyramid indenter with 136° phase angle. Flatly polished specimens were loaded at 200 gf with dwell time of 10 s. The average of five HV test values is reported herein. The specimens were tested according to ISO 6507/ASTM E 384 standards.

A Rockwell hardness (HR) test was conducted using a universal hardness testing machine (INNOVA, 783D) on metallographically polished samples. The macrohardness of the specimen was calculated on the HR15T scale from a test machine equipped with a 1/16-inch-diameter HM ball indenter. The dwell time used in the experiment was 10 s. The tests were conducted according to the ISO 6508/ASTM E 18 standards. The mean of five test values of HR is reported herein.

RESULTS AND DISCUSSION

X-ray Diffraction Analysis

The x-ray diffraction characterization technique was used to investigate the effect of TiB_2 on the crystallographic nature of the pure Mg matrix. The Mg-2.5TiB_2 composite could form due to the good wettability between the Mg matrix and TiB_2 reinforcement.[55] The Mg basal texture may be altered by the interaction of the TiB_2 reinforcement with its crystallographic structure.[56] The normalized XRD patterns of pure Mg, pure TiB_2, milled Mg-2.5TiB_2 composite, and spark-plasma-sintered composite samples are depicted in Fig. 1, where highly prominent individual peaks of Mg and TiB_2 powder can be seen clearly. However, in the case of the Mg-2.5TiB_2 composite, only the prominent peaks of Mg can be seen easily. This result is because TiB_2 is present at a relatively low weight percent (< 3 wt.%), meaning that the corresponding peaks are visible but with lower intensity. Moreover, the presence of TiB_2 in the synthesized composite is confirmed by the results for the spark-plasma-sintered sample at elevated temperatures. The first peak of TiB_2 at $2\theta = 27.94°$ can be observed in the samples sintered at 500°C and 550°C. The other peaks might be seen with relatively low intensities. It can be concluded that no extra peaks were observed in the XRD spectrum of these spark-plasma-sintered samples, confirming the absence of any extra phases formed during the sintering process. This result also establishes that the SPS process can be successfully used to produce Mg-2.5TiB_2 composites.

SEM Characterization

The SEM micrographs provide qualitative analysis of the particle morphology and shape of the as-received Mg (Fig. 2a), TiB_2 (Fig. 2b), and milled powder mixtures (Fig. 2c). Both as-received

powders showed irregular shape with a wide size distribution. The secondary-electron image in Fig. 2a shows that the Mg matrix consisted of particles with a wide size distribution, while Fig. 2b presents a more uniform particle size for the TiB_2 reinforcement. In addition, no large particles due to agglomeration could be seen, and this effect was even less noticeable after conventional sintering along with cold compaction.

The FE-SEM micrographs of the spark plasma sintered samples revealed a reasonable distribution

Fig. 1. X-ray patterns of as-received powders, milled, and SPS samples.

of the reinforcement in the matrix. FE-SEM images of the samples after SPS revealed no visible porosity. This result confirms the ability of the spark plasma sintering process to produce dense samples. FE-SEM micrographs also showed a reasonable distribution of TiB_2 in the Mg matrix with improved interfacial integrity. The improved interfacial integrity between the matrix and reinforcement resulted in the absence of debonding or voids in all the sintered samples. The absence of micropores or shrinkage in the Mg-2.5TiB_2 composites could also be noted from the micrographs. Figure S1 depicts FE-SEM micrographs of all the Mg-2.5TiB_2 samples. A reasonable TiB_2 reinforcement distribution can be seen clearly. The reinforcement exhibits a stable position within the matrix, confirming their strong adhesion. This strong adhesion of the reinforcement will provide adequate resistance to the indentation of Mg-2.5TiB_2 composites compared with the pure Mg matrix.

The crystallite size for the Mg powder, TiB_2 reinforcement, and sintered samples of the developed composites was calculated using the Scherrer equation. The crystallite size of the Mg powder and TiB_2 reinforcement was found to be ~ 36 nm and ~ 40 nm, respectively. However, variation of the different sintering parameters resulted in crystallite sizes in the range from ~ 30 nm to 42 nm for the sintered Mg-2.5 wt.%TiB_2 composite samples. This small variation in the crystallite size indicates minimal or no grain growth during the spark plasma sintering process.

Influence of Input Parameters on Microhardness

The aim of this experiment is to identify the most influential factors and their combinations affecting the microhardness of the Mg-2.5TiB_2 composites. The L_9 OA of the Taguchi design and measured microhardness are presented in Table I. A total of nine experiments were carried out to investigate the influence of uncontrollable parameters in terms of
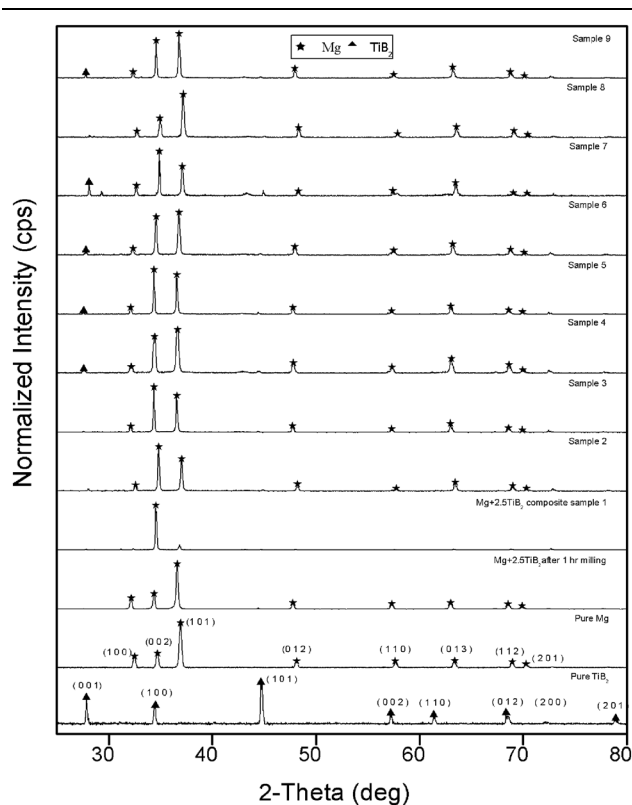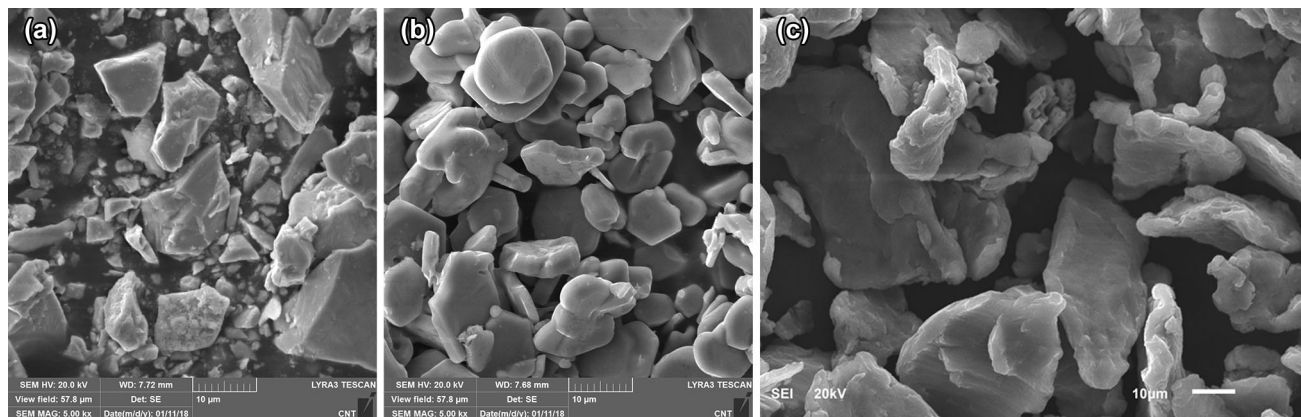

Fig. 2. SEM micrographs of as-received Mg (a), as-received TiB_2 (b), and as-milled (c) composite powder.

the S/N ratio on the sintering process, with each experiments being replicated at least five times. The main effect plots for the mean microhardness are shown in Fig. 3a, while the confirmation of the results based on the S/N ratio is presented in Supplementary Fig. S2. These plots depict the average values from each individual experiment and can be used to effectively investigate the effect of the factors on the mechanical properties. It can be easily inferred from Table II that the sintering temperature of 500°C resulted in the highest microhardness. Addition of the harder TiB_2 reinforcement enhanced the hardness of the Mg matrix due to localized matrix deformation during indentation. The increase of the microhardness at 500°C compared with 450°C can be attributed to an enhancement in the densification, as depicted in Fig. S1. By increasing the SPS temperature, the rate of bore eliminations increased, hence enhancing the density and hardness.[32,41]

However, at 550°C, the microhardness of the composite seemed to be lower. This result can be attributed to grain growth at high temperatures.[32,41] The effect of the sintering pressure can also be observed, with a high pressure of 50 MPa or more resulting in the occurrence of plastic deformation, leading to smaller grain size and high microhardness. The influence of the sintering time is similar to that of the sintering temperature, viz. long sintering time of 15 min resulted in grain growth and led to lower microhardness.

ANOVA was performed to investigate the relative influence of the process parameters on the microhardness. The ANOVA technique tests the difference between two or more means by variance analysis. This technique was carried out using Minitab 16 software at a 95% confidence interval (significance level $\alpha = 0.05$), and the results are presented in Supplementary Tables SI and SII. Table SI provides a summary of the ANOVA for microhardness, which is confirmed by the ANOVA results for the S/N ratio in Supplementary Table SII.

In Table SI, all the sintering parameters have a p value less than 0.05, which indicates that all the parameters had a strong influence on the microhardness of the Mg-2.5TiB_2 composite. The sintering temperature with a p value of 0.001 is the most statistically significant sintering parameter, followed by the sintering time and sintering pressure, with p values of 0.005 and 0.007, respectively, exhibiting statistical significance. It can easily be inferred that the measured microhardness was profoundly affected by all the sintering parameters.

The p value in ANOVA can be used to check the significance of a variable in a process. It may also be used to indicate interaction patterns among variables. A lower p value indicates a more significant influence of a variable on the process. Besides, the F value and sum of squares can also help to identify the most significant factor. Generally, factors with high F values and sum of squares are the most

significant. The ranking of the sintering parameters in terms of achieving the optimum mean microhardness and mean S/N ratio is also shown by the ANOVA. The degree of freedom (DoF) represents the number of independent values in the final test statistic calculation. The sequential sum of squares (Seq SS) represents the reduction in the error sum of squares when introducing one or more independent variables into the regression model. The Seq SS is used to check whether one or more than two but less than all the slope parameters are zero. The adjusted sum of squares (Adj SS) is used to measure the variation in various parts of the model or terms and then calculate the p value. The adjusted mean square (Adj MS) is responsible for measuring the extent of variation in a term or model, and Minitab uses it to measure the p value.

Influence of Input Parameters on Macrohardness

The L_9 OA for the macrohardness measured from the Rockwell test on the HR15T scale is presented in Table III. The results of the ANOVA for macrohardness are presented in Supplementary Table SIII, while the confirmation of the results for the S/N ratio and ranking of factors is presented in Supplementary Table SIV. The main effect plots for the average macrohardness are depicted in Fig. 3b, while the main effect plots for the S/N ratio to confirm the results are shown in Fig. S3. A slight variation in the macrohardness between 450°C and 500°C can be observed, and its value decreased significantly with a further increase in sintering temperature, reaching a minimum value of 37.872 HR. This result can be ascribed to the higher grain growth at high temperatures. The Hall–Petch relationship is applicable when the macrohardness decreases with increase in the grain size.[57] The increase in the material temperature enhanced the migration and annihilation of dislocations, which reduced the dislocation density. Thus, the number of grains per grain boundary decreased, resulting in a larger grain size. With an increase in the sintering pressure, the plastic deformation increases, leading to higher plastic deformation and a higher number of dislocations and dislocation density. Thus, a higher number of dislocations resulted in a smaller grain size, thereby increasing the macrohardness. However, pressure of more than 40 MPa with longer sintering time resulted in larger grain size and, therefore, the opposite effect. Also, the influence of the sintering time on the macrohardness of Mg-TiB_2 is paramount and increases with increasing heating time. The maximum value of 60.248 HV was obtained after sintering for 10 min, whereas a further increase in time resulted in a significant reduction in macrohardness. This result may be due to high grain growth, which occurred due to the high exposure time under elevated temperatures.
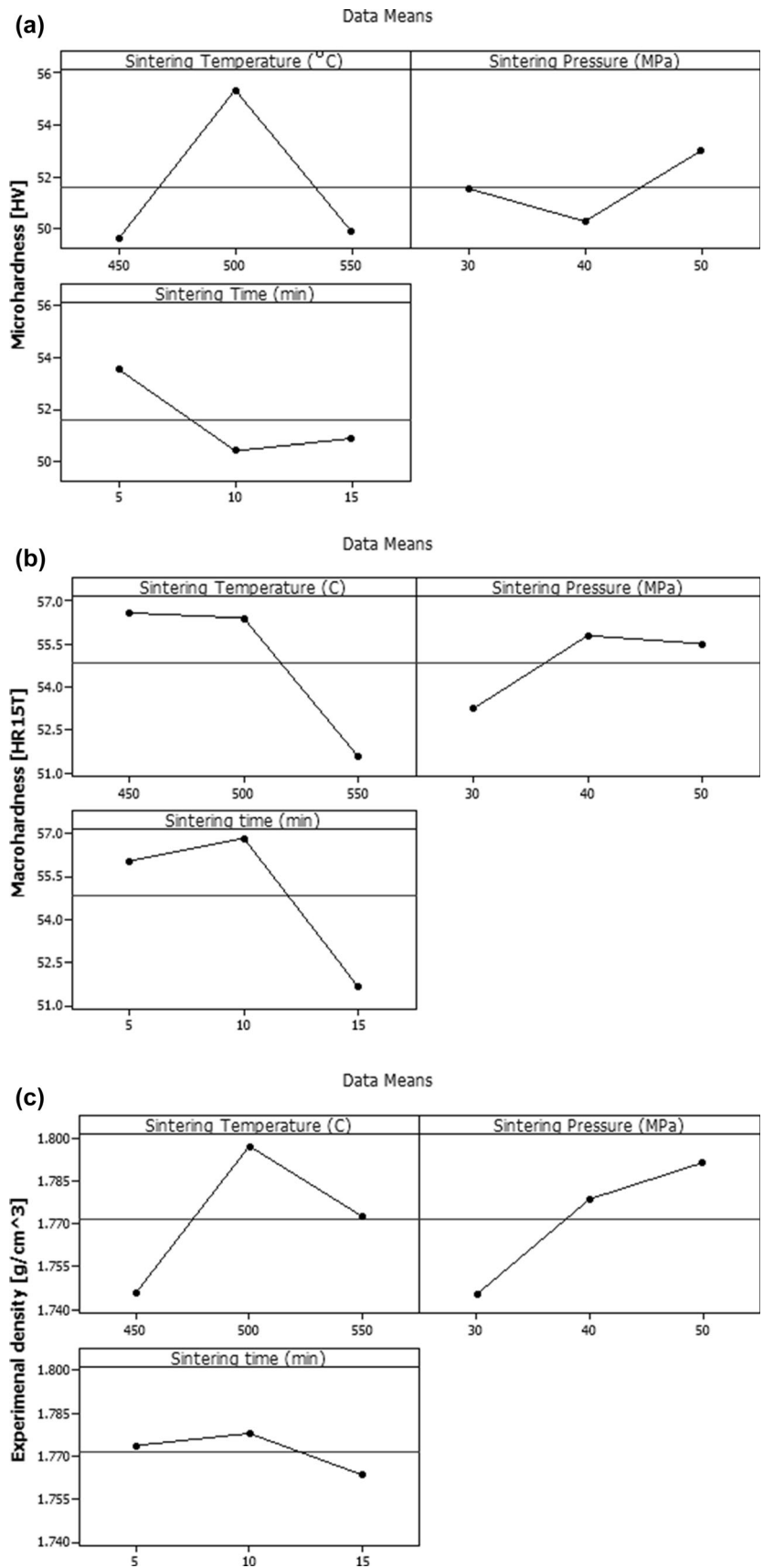
Fig. 3. Effect of SPS processing parameters on microhardness (a), macrohardness (b), and experimental density (c).

Table II. Experimental results according to sintering parameters for the mean microhardness and S/N ratio

Experimental run	Sintering parameters			Responses [microhardness (HV), S/N ratio (dB)]	
	S. Temp (°C)	S. Pres (MPa)	S. Time (min)	Mean MH (HV)	Mean S/N ratio (dB)
1	450	30	5	51.4	34.2139
2	450	40	10	47.0	33.4420
3	450	50	15	50.4	34.0486
4	500	30	10	54.2	34.6800
5	500	40	15	53.2	34.5182
6	500	50	5	58.6	35.3580
7	550	30	15	49.0	33.8039
8	550	40	5	50.6	34.0830
9	550	50	10	50.0	33.9794

Table III. Experimental results according to sintering parameters for the mean macrohardness and S/N ratio

Experimental run	Sintering parameters			Responses [macrohardness (HR15T), S/N ratio (dB)]	
	S. Temp (°C)	S. Pres (MPa)	S. Time (min)	Mean MH (HR)	Mean S/N ratio (dB)
1	450	30	5	62.186	35.8739
2	450	40	10	50.626	34.0875
3	450	50	15	56.852	35.0949
4	500	30	10	59.612	35.5067
5	500	40	15	60.184	35.5896
6	500	50	5	49.364	33.8682
7	550	30	15	37.872	31.5664
8	550	40	5	56.518	35.0437
9	550	50	10	60.248	35.5989

Influence of Input Parameters on Density

The L_9 orthogonal array based on the Taguchi design for the experimental density (ED) measured using Archimedes' principle is presented in Table IV, along with the S/N ratio. Besides, the theoretical density (TD) of the composite and standard deviation of the density values are also presented in Table IV.

The main effect plots for the average density are depicted in Fig. 3c, while Fig. S4 presents the S/N ratio. The density increased with increasing sintering temperature and then subsequently decreased with a further increase in sintering temperature, as can be observed in Fig. 3c. This typical behavior can be ascribed to the melting and enhanced diffusion of solid particles leading to the porosity minimization for the Mg-2.5TiB$_2$ composite at 500°C. However, a further increase in the sintering temperature to 550°C increased the volume of the prepared composite and eventually decreased the density. The increased density of the composite could also be attributed to the higher density (4.52 g/cm^3) of the TiB$_2$ reinforcement.[12] It can be inferred from the

higher density that the SPS consolidation process used in this study can be used to fabricate dense materials. The standard deviation on the density was very low at 500°C, revealing the reasonably good distribution of the TiB$_2$ reinforcement in the Mg matrix. The minimum porosity of 0.23% could easily be achieved when using the specific parameter values in Table IV in the novel SPS consolidation technique. It can also be observed from Fig. 3c that the experimental density of the composites increased with increasing sintering pressure. This result can be attributed to the decrease in the volume of the solid composite powder. Besides, an increase in the pressure during sintering filled the intergranular pores and led to a higher density. The influence of the sintering time on the experimental density of Mg-2.5TiB$_2$ is similar to that of sintering temperature, with a slight abrupt variation. At the beginning, the density was lower due to insufficient diffusion and higher porosity due to interparticle voids. However, at 10 min sintering time, the diffusion was sufficient to fill the existing pores and increase the experimental density without any

Table IV. Experimental results according to sintering parameters for the mean density and S/N ratio

	Sintering parameters					Responses [experimental density (g/cm^3), S/N ratio (dB)]		
Experimental run	S. Temp (°C)	S. Pres (MPa)	S. Time (min)	TD (g/cm^3)	Mean ED (g/cm^3)	SD	Porosity (%)	Mean S/N ratio (dB)
1	450	30	5	1.80	1.72	0.035766	4.56	4.73616
2	450	40	10	1.80	1.74	0.002109	3.56	4.82659
3	450	50	15	1.80	1.76	0.025827	2.164	4.95174
4	500	30	10	1.80	1.78	0.003174	1.06	5.04904
5	500	40	15	1.80	1.79	0.000411	0.44	5.10269
6	500	50	5	1.80	1.80	0.001625	0.25	5.11975
7	550	30	15	1.80	1.72	0.014248	4.74	4.71976
8	550	40	5	1.80	1.79	0.000656	4.56	5.07016
9	550	50	10	1.80	1.80	0.001819	3.56	5.11513

variation or with minimal variation in the volume. However, a further increase in the sintering time to 15 min exposed the composite material to high temperature for a longer time. This led to a higher volume of the composite, and eventually, the density was reduced. The results obtained from the ANOVA test for the experimental density are presented in Supplementary Table SV, while the analysis for the S/N ratio is presented in Supplementary Table SVI. By examining the p value for all the process parameters and the S/N ratio, it can be inferred that none of the factors contributed significantly to the variation in the experimental density of the Mg-2.5TiB$_2$ microcomposite, because the p value for each factor is greater than the confidence interval of 5%. The sintering temperature, pressure, and time were all negligible factors. However, the sintering pressure and time were dominant among the least negligible factors affecting the variation in the experimental density. The sintering temperature with a p value of 0.229 was the least influential of the negligible factors influencing the composite experimental density.

CONCLUSION

A magnesium-based metal matrix composite was fabricated using spark plasma sintering (SPS). The Taguchi design approach was used to analyze the significance of the influence of the sintering temperature, pressure, and time on the physical and mechanical properties of the Mg-based composites.

The following conclusions can be drawn from this work:

1. A magnesium-based metal matrix composite reinforced with 2.5 wt.% TiB$_2$ was successfully developed by the spark plasma sintering technique.
2. Microstructural analysis revealed no visible porosity in FE-SEM micrographs and showed a reasonably homogeneous distribution of TiB$_2$ in the Mg matrix. The hardness values increased with inclusion of the TiB$_2$ reinforcement compared with the pure Mg matrix.
3. The microhardness was significantly influenced by all the sintering parameters. The sintering temperature was the most dominant factor affecting the microhardness, closely followed by the sintering time and pressure.
4. None of the sintering parameters made a significant contribution to the macrohardness of the fabricated composite.

ELECTRONIC SUPPLEMENTARY MATERIAL

The online version of this article (https://doi.org/10.1007/s11837-019-03997-5) contains supplementary material, which is available to authorized users.

REFERENCES

1. R. del Campo, B. Savoini, A. Muñoz, M.A. Monge, and G. Garcés, *J. Mech. Behav. Biomed. Mater.* 39, 238 (2014).
2. E.P. DeGarmo, J.T. Black, R.A. Kohser, and B.E. Klamecki, *Materials and Process in Manufacturing*, 9th ed. (Upper Saddle River: Prentice Hall, 1997).
3. G. Garcés, M. Rodríguez, P. Pérez, and P. Adeva, *Compos. Sci. Technol.* 67, 632 (2007).
4. M. Ali, M. Hussein, and N. Al-Aqeeli, *J. Alloys Compd.* 792, 1162 (2019).
5. S.F. Hassan and M. Gupta, *J. Alloys Compd.* 345, 246 (2002).
6. X.N. Gu, X. Wang, N. Li, L. Li, Y.F. Zheng, and X. Miao, *J. Biomed. Mater. Res. Part B Appl. Biomater.* 99B, 127 (2011).

7. M. Rashad, F. Pan, M. Asif, J. She, and A. Ullah, *J. Magnes. Alloys* 3, 1 (2015).
8. G.K. Meenashisundaram, M.H. Nai, A. Almajid, and M. Gupta, *Mater. Des.* 65, 104 (2015).
9. S. Sankaranarayanan, U. Pranav Nayak, R.K. Sabat, S. Suwas, A. Almajid, and M. Gupta, *J. Alloys Compd.* 615, 211 (2014).
10. S.F. Hassan and M. Gupta, *Mater. Sci. Eng. A* 392, 163 (2005).
11. S.F. Hassan and M. Gupta, *J. Compos. Mater.* 41, 2533 (2007).
12. G.K. Meenashisundaram, S. Seetharaman, and M. Gupta, *Mater. Charact.* 94, 178 (2014).
13. M.P. Staiger, A.M. Pietak, J. Huadmai, and G. Dias, *Biomaterials* 27, 1728 (2006).
14. W.N. Tang, S.S. Park, and B.S. You, *Mater. Des.* 32, 3537 (2011).
15. F. Barrère, T.A. Mahmood, K. de Groot, and C.A. van Blitterswijk, *Mater. Sci. Eng. R Rep.* 59, 38 (2008).
16. S. Jaiswal, R.M. Kumar, P. Gupta, M. Kumaraswamy, P. Roy, and D. Lahiri, *J. Mech. Behav. Biomed. Mater.* 78, 442 (2018).
17. G. Eddy Jai Poinern, S. Brundavanam, and D. Fawcett, *Am. J. Biomed. Eng.* 2, 218 (2013).
18. M. Hussein, A. Mohamed, and N. Al-Aqeeli, *Materials* 8, 2749 (2015).
19. S. Kannan, A. Balamurugan, and S. Rajeswari, *Mater. Lett.* 57, 2382 (2003).
20. M. Niinomi, *Metall. Mater. Trans. A* 33, 477 (2002).
21. L. Li, J. Gao, and Y. Wang, *Surf. Coat. Technol.* 185, 92 (2004).
22. T.H.D. Ong, N. Yu, G.K. Meenashisundaram, B. Schaller, and M. Gupta, *Mater. Sci. Eng. C* 78, 647 (2017).
23. J. Umeda, M. Kawakami, K. Kondoh, E.-S. Ayman, and H. Imai, *Mater. Chem. Phys.* 123, 649 (2010).
24. M.H. Nai, J. Wei, and M. Gupta, *Mater. Des.* 60, 490 (2014).
25. C. Ma, L. Chen, J. Xu, A. Fehrenbacher, Y. Li, F.E. Pfefferkorn, N.A. Duffie, J. Zheng, and X. Li, *J. Biomed. Mater. Res. Part B Appl. Biomater.* 101B, 870 (2013).
26. H. Khoshzaban Khosroshahi, F. Fereshteh Saniee, and H.R. Abedi, *Mater. Sci. Eng. A* 595, 284 (2014).
27. A.K. Khanra, H.C. Jung, K.S. Hong, and K.S. Shin, *Mater. Sci. Eng. A* 527, 6283 (2010).
28. B. Chen, K.-Y. Yin, T.-F. Lu, B.-Y. Sun, Q. Dong, J.-X. Zheng, C. Lu, and Z.-C. Li, *J. Mater. Sci. Technol.* 32, 858 (2016).
29. E. Mohammadi Zahrani and M.H. Fathi, *Ceram. Int.* 35, 2311 (2009).
30. C.A. Stüpp, G. Szakács, C.L. Mendis, F. Gensch, S. Müller, F. Feyerabend, D. Hotza, M.C. Fredel, and N. Hort, *Magnesium Technology* (Cham: Springer, 2015), pp. 425–429.
31. M.H. Fathi and E.M. Zahrani, *J. Alloys Compd.* 475, 408 (2009).
32. M.A. Hussein, C. Suryanarayana, M.K. Arumugam, and N. Al-Aqeeli, *Mater. Des.* 83, 344 (2015).
33. Y.F. Zheng, X.N. Gu, Y.L. Xi, and D.L. Chai, *Acta Biomater.* 6, 1783 (2010).
34. V.A.R. Henriques, E.T. Galvani, S.L.G. Petroni, M.S.M. Paula, and T.G. Lemos, *J. Mater. Sci.* 45, 5844 (2010).
35. S.F. Hassan, *Arch. Metall. Mater.* 61, 1521 (2016).
36. P.S. Kumar, K. Ponappa, M. Udhayasankar, and B. Aravindkumar, *Arch. Metall. Mater.* 62, 1851 (2017).
37. H. Cay, H. Xu, and Q. Li, *Mater. Sci. Eng. A* 574, 137 (2013).
38. M. Rashad, F. Pan, A. Tang, Y. Lu, M. Asif, S. Hussain, J. She, J. Gou, and J. Mao, *J. Magnes. Alloys* 1, 242 (2013).
39. S.F. Hassan and M. Gupta, *Compos. Struct.* 72, 19 (2006).
40. M. Oghbaei and O. Mirzaee, *J. Alloys Compd.* 494, 175 (2010).
41. M.A. Hussein, C. Suryanarayana, and N. Al-Aqeeli, *Mater. Des.* 87, 693 (2015).
42. D. Salamon and Z. Shen, *Mater. Sci. Eng. A* 475, 105 (2008).
43. B. Yaman and H. Mandal, *Mater. Lett.* 63, 1041 (2009).
44. N. Gao, J. Li, D. Zhang, and Y. Miyamoto, *J. Eur. Ceram. Soc.* 22, 2365 (2002).
45. M. Omori, *Mater. Sci. Eng. A* 287, 183 (2000).
46. N.Q. Cao, D.N. Pham, N. Kai, H.V. Dinh, S. Hiromoto, and E. Kobayashi, *Metals (Basel)* 7, 358 (2017).
47. T. Chartier and A. Badev, *Handbook of Advanced Ceramics: Chapter 6.5. Rapid Prototyping of Ceramics* (Amsterdam: Elsevier, 2013).
48. K. Tee, L. Lu, and M.O. Lai, *J. Mater. Process. Technol.* 89–90, 513 (1999).
49. M. Wong and Y.C. Lee, *Surf. Coat. Technol.* 120–121, 194 (1999).
50. H.Y. Wang, Q.C. Jiang, Y. Wang, B.X. Ma, and F. Zhao, *Mater. Lett.* 58, 3509 (2004).
51. J. Davim and P. Aveiro, *Design of Experiments in Production Engineering* (Cham: Springer, 2016).
52. S. Mavruz and R. Oğulata, *Fibres Text. East. Eur.* 18, 78 (2010).
53. Ö. Küçük, T. Elfarah, S. Islak, and C. Özorak, *Metals (Basel)* 7, 352 (2017).
54. P. Sahoo, A. Pratap, and A. Bandyopadhyay, *Int. J. Ind. Eng. Comput.* 8, 385 (2017).
55. Z. Xiuqing, W. Haowei, L. Lihua, T. Xinying, and M. Naiheng, *Mater. Lett.* 59, 2105 (2005).
56. N. Stanford, D. Atwell, A. Beer, C. Davies, and M.R. Barnett, *Scr. Mater.* 59, 772 (2008).
57. Y. Xu, F. Gensch, Z. Ren, K.U. Kainer, and N. Hort, *Prog. Nat. Sci. Mater. Int.* 28, 724 (2018).